J. Fluid Mech. (2010), *vol.* 648, *pp.* 485–507.
doi:10.1017/S0022112009993211

Nonlinear interactions between a free-surface flow with surface tension and a submerged cylinder

R. M. MOREIRA† AND D. H. PEREGRINE‡
School of Mathematics, University of Bristol, University Walk, Bristol BS8 1TW, UK

(Received 1 January 2009; revised 2 November 2009; accepted 3 November 2009)

A submerged cylinder in a uniform stream flow is approximated by a horizontal doublet, following Lamb's classical method. A linear steady solution including surface tension effects is derived, showing that under certain conditions small-scale ripples are formed ahead of the cylinder, while a train of 'gravity-like' waves appear downstream. Surface tension effects and a dipole are included in the fully nonlinear unsteady non-periodic boundary-integral solver described by Tanaka *et al.* (*J. Fluid Mech.*, vol. 185, 1987, pp. 235–248). Nonlinear effects are modelled by considering a flat free surface or the linear stationary solution as an initial condition for the fully nonlinear irrotational flow programme. Long-run computations show that these unsteady flows approach a steady solution for some parameters after waves have radiated away. In other cases the flow does not approach a steady solution. Interesting features at the free surface such as the appearance of 'parasitic capillaries' near the crest of gravity waves and the formation of capillary–gravity waves upstream of the cylinder are found.

1. Introduction

The study of gravity waves formed at a free surface by the flow of a uniform stream interacting with a submerged cylinder has attracted the interest of researchers since the early 20th century. Kelvin was perhaps the first to suggest that problem in 1905, followed by Lamb who analysed it formally in the light of linear water wave theory in 1913 (for a more accessible version of this paper see Lamb 1932, § 247). Lamb's method consisted of replacing the cylinder by the equivalent doublet at its centre and then finding the fluid motion due to this doublet. Supposing a steady irrotational potential flow with a linearized free-surface boundary condition, he found the appearance of a local disturbance immediately above the obstacle followed by a train of stationary sinusoidal gravity waves on the downstream side (see figure 1). This solution is applicable when the cylinder is of small radius compared with the depth of its axis; then the disturbance to the free stream due to the presence of the cylinder causes small-amplitude waves that can be approximated by linear theory.

† Present address: Computational Fluid Dynamics Laboratory, Fluminense Federal University, Rua Passo da Pátria 156, bl.D, sl.563A, Niterói, RJ 24210-240, Brazil. Email address for correspondence: roger@vm.uff.br.

‡ Professor Peregrine passed away before this paper was completed. This manuscript was prepared for publication by the first author.

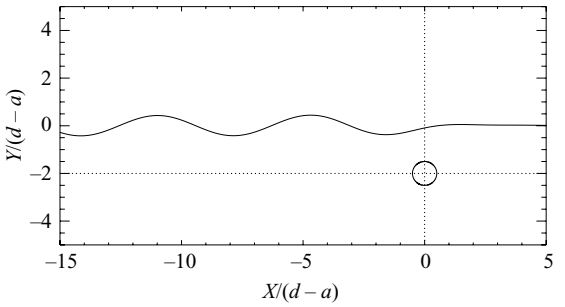

FIGURE 1. Stationary linear waves due to the presence of a cylinder of radius a and depth d of submergence on a uniform stream flow U, with surface tension effects neglected; $a/d = 1/4$, $U = -1$.

Havelock (1926) carried out further approximations for the free-surface gravity flow in the vicinity of an approximately circular cylinder in a uniform stream by the method of successive images, with a first-order free-surface condition. He reported that the accuracy of the first-order approximation for the surface elevation increases rapidly as the depth of submergence increases or as we take relatively smaller velocities. In a following paper, Havelock (1936) used a set of multipoles – the first of which is just the dipole in Lamb's method – from which an exact circular cylinder condition was applied.

Investigations on the importance of nonlinear effects from the free-surface boundary condition were carried out by Tuck (1965), who emphasized that a simple linearization would be inadequate for cases in which the cylinder is close to the free surface, whereas it does not satisfy the assumption $a/d \ll 1$ (with a and d representing the radius and the depth of submergence of the centre of the cylinder). He suggested that the exact nonlinear solution would involve highly non-sinusoidal or even breaking waves. Tuck (1965) also claimed that there is no need for all the extra terms in the series proposed by Havelock (1936) – Lamb's submerged dipole is a good approximation – since nonlinearities have a more important effect than satisfying the cylinder boundary condition exactly.

Following the work of Tuck (1965), Dagan (1971) investigated the free-surface gravity flow past a submerged cylinder at high Froude number by the method of matched asymptotic expansions. A good agreement with linear theory was found for deep-submerged bodies; for a body close to the free surface the nonlinear calculations differed significantly from the linearized solution. Other authors who have more recently studied free-surface gravity flows generated by submerged cylinders include Scullen & Tuck (1995) and Tyvand & Miloh (1995*a*,*b*).

All the works described above were carried out neglecting the effects of surface tension on the free-surface flow. For large-scale surface disturbances (of length greater than 10 cm) this approximation is adequate; gravity is dominant, and in the absence of wind the pressure exerted on the surface by the atmosphere can be considered constant. At a small scale, however, the surface pressure can be modified by surface tension. Capillary phenomena may arise when the surface possesses considerable curvature or when surface tension gradients appear on that surface. In both cases, the presence of these forces changes the nature of the free-surface flow or induces motion that is originally absent.

Several authors described the existence of small-scale ripples or capillary waves upstream of a local disturbance as well as larger gravity waves downstream of it

(Forbes 1983; Milewski & Vanden-Broeck 1999; Grandison & Vanden-Broeck 2006). Such situation may occur for a general disturbance, which may take the form of a step in the bed or of a cylindrical obstacle situated on the bed, in the midst of the water or on the surface of a stream flow. The incoming stream has a speed exactly equal to the phase velocity of the generated waves. Since the group velocity of the capillary waves is greater than their phase velocity, they appear ahead of the generating object.

The theoretical approach most applied to the understanding of these waves rests on the linear theory of a point pressure disturbance of a steady stream, presented by Lamb (1932, §§270 and 271; see also Whitham 1999, p. 452). Lamb (1932) showed that there are several possible solutions to the problem, depending upon whether the stream velocity is greater, less than or equal to the waves' minimum phase velocity. The results show that wave amplitudes are known functions of the motion of the obstacle. The calculated asymptotic wavetrains confirm the results obtained from group velocity concepts: gravity waves are formed downstream, while capillary waves appear upstream of the obstacle.

The dynamical theory of the generation of capillary waves and their interaction with gravity waves has been developed by Longuet-Higgins (1963), Crapper (1970) and Ruvinsky & Freidman (1981). Since then, numerical simulations have become a powerful tool in the understanding of such flows, and several publications on this subject can be found (Ruvinsky, Feldstein & Freidman 1991; Jervis 1996; Ceniceros & Hou 1999). These works deal with length scales where gravity is the dominant restoring force but with surface tension remaining locally important in regions of high curvature. The study of the solution space for two-dimensional symmetric capillary–gravity waves has also attracted many researchers during the past years. Solutions corresponding to families of travelling periodic waves and solitary waves have been found. These correspond to length scales where both surface tension and gravity are important. This problem is of interest not only because the waves are steep but also because the solutions become singular when close to the minimum phase velocity. The varied physical aspects of gravity–capillary waves can be found in the review papers of Dias & Kharif (1999) and Perlin & Schultz (2000).

Wilton's ripples represent a classical solution that contains apparent singularities. Wilton (1915) presented a fifth-order Stokes expansion of the surface profile when studying periodic capillary–gravity waves of finite amplitude in the vicinity of the minimum of the dispersion relation. He noticed that the perturbation expansion has zero radius of convergence at certain wavelengths and reformulated the expansion, finding that two possible waves can exist at the shortest of these wavelengths, with the wavelength given by the capillary branch being an integral divisor of the wavelength given by the gravity branch. Since the primary wave interacts resonantly with one of its higher harmonics, the perturbation method fails. It was thought that no solutions existed at these wavelengths, in real applications the effect being reduced by viscosity. Further contributions to the theme have been published more recently by Vanden-Broeck (2002).

Much work has since concentrated on the failure of the perturbation expansion at these wavelengths (see Hogan 1979). Further unexpected results for capillary–gravity waves, such as a rapid decrease with increasing wave height of the gravitational potential energy, were then found by Hogan (1981). This decrease was connected with an extreme distortion of the free-surface profile. Different approaches to the problem of calculating finite-amplitude capillary–gravity waves of permanent form on the surface of an inviscid incompressible irrotational fluid have also been proposed.

Authors who have written on the subject include Hogan (1979, 1980, 1981), Schwartz & Vanden-Broeck (1979), Rottman & Olfe (1979) and Chen & Saffman (1980). They have shown that there is a multiplicity of solutions for any set of parameter values. In particular, Maleewong, Grimshaw & Asavanant (2005) showed that many different families of capillary–gravity waves exist for Bond numbers between 0 and 1/3 (for its definition, see (2.11) below).

Hogan (1983) found abrupt changes in the sign of the energy flux for a small increase of wave amplitude when estimating the energy flux of capillary–gravity waves in a moving stream for various wavelengths as a function of the wave amplitude. He concluded that 'gravity-like' waves may jump from downstream to upstream when the velocity of the stream approaches the minimum phase speed in the gravity branch. Oppositely, 'capillary-like' waves would change from upstream to downstream when the velocity of the stream approaches the minimum phase speed in the capillary branch. A possible experiment was suggested in order to observe these jumps.

Linear results are restricted to a region in which the amplitude of the disturbances are significantly small, thus satisfying the inequality $a/d \ll 1$. As the ratio a/d increases, the roughness of the free surface is augmented and waves become 'steeper', with nonlinear effects taking over. The implications of the nonlinear results for experimental observations are not completely clear. The current paper reports an investigation of the effects of nonlinearity and surface tension at the free surface when a steady stream flow interacts with a submerged cylinder. A version of the fully nonlinear non-periodic boundary-integral method described by Tanaka *et al.* (1987) and modified for the inclusion of surface tension by Jervis (1996) is adapted to this situation. The current work has focused on a general investigation of the capillary–gravity waves that may be produced upstream and downstream of the cylinder, especially in the region in which the linear solutions become singular.

2. Governing equations

2.1. *Unsteady nonlinear model*

To model fully nonlinear effects at a free surface in a spatially non-periodic domain, the boundary-integral scheme described by Tanaka *et al.* (1987) is used as its starting point. An extension of the method which includes the modelling of unsteady free-surface flows with surface tension implemented by Jervis (1996) is used to investigate the effects of surface tension. Following Lamb's classical method, the numerical scheme is adapted to include a horizontal doublet in a uniform stream flow defined by $\boldsymbol{U} = (U, 0)$. The fluid flow is assumed to be inviscid and incompressible with the single doublet located below the free surface at a depth d of submergence. It is also assumed that the flow is irrotational outside the singular core and away from the free surface. The irrotational velocity field $\boldsymbol{u}(x, y, t)$ is then given by the gradient of a velocity potential $\Phi(x, y, t)$ which satisfies Laplace's equation in the fluid domain, excluding the singular point. All the interior properties of the fluid are then determined by its properties at the boundaries alone. The entire motion can be modelled by considering a point discretization of the surface. The solution method is based on solving an integral equation that arises from Cauchy's integral theorem for functions of a complex variable.

In order to apply Cauchy's integral theorem to the problem, the potential Φ must be known on all the boundaries. The kinematic and dynamic boundary conditions

are applied at the free surface such that

$$\frac{\mathrm{D}\boldsymbol{r}}{\mathrm{D}t} = \nabla\Phi, \qquad \frac{\mathrm{D}\Phi}{\mathrm{D}t} = \frac{1}{2}\,|\nabla\Phi|^2 - gy - \frac{p}{\rho}, \tag{2.1}$$

where $\boldsymbol{r} = (x, y, t)$; y is the elevation of the free surface above the undisturbed water level; g is the acceleration due to gravity; and ρ is the fluid density. In the presence of surface tension, the pressure p exerted at the free surface is given by

$$p = p_0 - \tau\frac{\partial^2\eta}{\partial x^2}\left[1 + \left(\frac{\partial\eta}{\partial x}\right)^2\right]^{-3/2}, \tag{2.2}$$

where τ is the surface tension coefficient; p_0 is the pressure on the exterior side of the surface and can be chosen to approximate the effects of wind or a localized pressure on the surface, though it is not used in the calculations. The last term in (2.2) refers to the contribution of surface tension effects to the pressure p which depends on the curvature of the free surface, defined by $y = \eta(x, t)$.

The fluid domain must be of finite extent in x for the purpose of computing a numerical solution. We approximate the desired 'infinite' domain by assuming a finite extension in x that goes from, namely, $-X_\infty$ to X_∞, which satisfies the criterion

$$|\nabla\Phi(\pm X_\infty, y, t) - \boldsymbol{U}| < \varepsilon, \tag{2.3}$$

valid for $-\infty < y \leqslant 0$ and $t > 0$; ε is a specified small 'precision' parameter, while $\nabla\Phi(\pm X_\infty, y, t)$ is evaluated as explained in Dold (1992). For any time t, $\pm X_\infty$ are then determined iteratively by the numerical scheme; 10 equally spaced points are added to the far ends of the free surface until criterion (2.3) is fully satisfied. Thus the distance between $-X_\infty$ and X_∞ is expected to increase with time because of the propagation of disturbances to the far field. It is also assumed that the water is deep, satisfying the condition $\nabla\Phi \to (U, 0)$ as $y \to -\infty$. To complete the model, an initial condition for the free surface is required such that $\eta(x, t) = \eta_0(x, 0)$ and $\Phi(x, \eta, t) = \Phi_0(x, \eta_0, 0)$. The numerical computations consider a flat free surface or the linear steady free-surface profile derived in the following section as the initial condition for the fully nonlinear unsteady problem.

The introduction of a horizontal doublet in our model is done by decomposing our velocity potential Φ into a regular part ϕ_w (due to surface waves) and a singular part ϕ_s (due to the singularity) such that $\Phi = \phi_w + \phi_s$ (for more details, see Moreira 2001). The velocity potential ϕ_s is then given by the real part of the complex potential for an irrotational flow due to an approximately circular cylinder held in a stream with uniform velocity U far from the cylinder (see Batchelor 1967, p. 424). To apply Cauchy's integral theorem to the non-periodic free-surface flow problem in deep water, the complex potential ω includes for convenience the reflection of the cylinder in the free surface,

$$\omega(z) = U\left(z - z_0 + \frac{a^2}{z - z_0} + \frac{a^2}{z - \bar{z}_0}\right), \tag{2.4}$$

where $z = x + \mathrm{i}y$ and $z_0(= x_0 + \mathrm{i}y_0)$ is the position of the centre of the cylinder, $\bar{z}_0$ its complex conjugate and a the radius of the cylinder.

Basically the method of solution consists of the following stages. Initially the velocity potential Φ is known on the surface for each time step. The potential ϕ_s due to the dipole is subtracted from the surface value of Φ such that the remaining surface wave potential ϕ_w, which has no singularity in the fluid domain, can be used with

Cauchy's integral theorem to calculate the velocity $\nabla\phi_w$ on the free surface. Then the potential ϕ_s is added back in, and the corresponding 'total' velocities are evaluated. The free surface is stepped in time, using a truncated Taylor series. Such stages are repeated until either the final time is reached, or the algorithm breaks down. The calculation of higher-order time derivatives of ϕ_w necessitates the computation of higher time derivatives of the surface pressure p defined by (2.2). This is how surface tension effects come into the numerical scheme. For a constant surface pressure ($p = p_0$), all time derivatives with respect to p become zero.

Regarding stability, the numerical code is occasionally susceptible to sawtooth modes. Such instabilities feature in most existing numerical schemes that follow the motion of surface gravity waves and were first reported by Longuet-Higgins & Cokelet (1976), who employed smoothing techniques to control them. Dommermuth (2000) has also shown that spurious high-frequency standing waves are generated when numerical simulations of nonlinear progressive waves are initialized using linear waves in high-order spectral methods. If present, these unstable modes are mostly eliminated by restricting the maximum size of time step and/or by taking higher orders of backward differencing. Otherwise one of the several smoothing polynomial formulae given by Dold (1992) effectively removes the unstable modes that may eventually appear. In all the computations involving pure gravity waves presented in the current paper, smoothing was not necessary.

With the introduction of surface tension, sawtooth numerical instabilities appear more frequently in the surface variables. The source of these unstable modes resides in the calculation of the capillary wave pressure and its Lagrangian derivatives, which would eventually cause the breakdown of computations. A sufficient number of surface calculation points is then necessary in order to have any capillary wave well resolved and thus not being smoothed away by the numerical scheme. If necessary a low-order smoothing formula is employed. This proves to be efficient in the removal of unstable modes and also gives a slightly larger maximum steepness of surface waves rather than when employing a higher-order formula.

2.2. *Linear theory*

From the theory of linear water waves and supposing that the surface waves propagate in deep water, surface tension effects are included in the dispersion relation such that the phase speed c satisfies

$$c(k) = \left(\frac{g}{k} + \frac{\tau}{\rho}k\right)^{1/2}, \tag{2.5}$$

where k is the wavenumber. (For the purpose of calculations, we suppose $g = 980.6$ cm s^{-2}, $\tau = 74.0$ g s^{-2} and $\rho = 1.0$ g cm^{-3}.) The group velocity c_g of the surface waves are related to k by

$$c_g(k) = \frac{c}{2}\left(\frac{\rho g + 3\tau k^2}{\rho g + \tau k^2}\right). \tag{2.6}$$

The linear dispersion relation represented by (2.5) has a minimum value at

$$k = k_m = \left(\frac{\rho g}{\tau}\right)^{1/2}, \qquad c = c_m = \left(\frac{4g\tau}{\rho}\right)^{1/4}, \tag{2.7}$$

while the minimum group velocity is attained at $k = k_{g_m} = 0.40k_m$ and $c_g = c_{g_m} = 0.77c_m$. Here we define k_{g_m} and c_{g_m} as the wavenumber and speed at the minimum group velocity. For convenience expressions (2.5) and (2.6) are non-dimensionalized

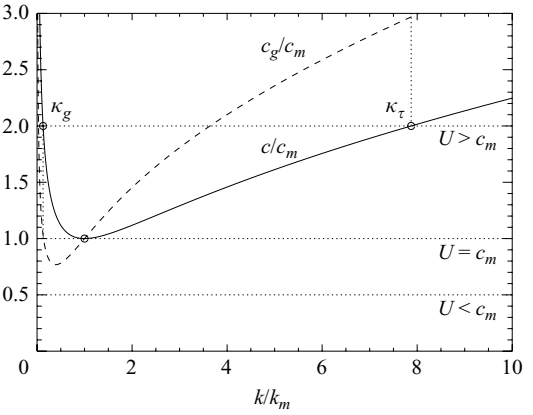

FIGURE 2. Phase speed and group velocity of capillary–gravity waves in deep water as a function of wavenumber, in units of c_m and k_m.

in terms of k_m and c_m, reducing to

$$\frac{c}{c_m} = \left[\frac{1}{2}\left(\frac{k}{k_m} + \frac{k_m}{k}\right)\right]^{1/2}, \qquad \frac{c_g}{c_m} = \frac{1}{2}\frac{c}{c_m}\left[\frac{(k_m/k)^2 + 3}{(k/k_m)^2 + 1}\right]. \tag{2.8}$$

The graphs of c and c_g against k in units of c_m and k_m are shown in figure 2.

The waves produced by an obstacle on a uniform stream flow U may be viewed as the waves produced by the same obstacle moving with speed $-U$. In this frame of reference, supposing a two-dimensional problem, the only stationary waves that can keep up with the obstacle must satisfy the relation

$$c(k) = U. \tag{2.9}$$

Therefore, if $U > c_m$, two solutions are possible, one coming from the gravity branch, namely k_g, and the other from the capillary branch k_τ, such that $k_g < k_\tau$. These solutions can be associated to the group velocity through expression (2.8) such that

$$c_g(k_g) < c(k_g), \qquad c_g(k_\tau) > c(k_\tau). \tag{2.10}$$

Since $c(k_g) = c(k_\tau) = U$, the capillary waves have a group velocity bigger than the stream velocity and therefore must appear ahead of the obstacle. The gravity waves must be downstream, since their group velocity is slower than U.

When the stream velocity U is close to the minimum phase velocity c_m, the group velocity c_g is very close to U, and the energy can move away from the pressure source only very slowly. As we approach c_m, a significant increase in wave steepness is associated to the linear solution, and nonlinear effects start to become important. (Expressions for the linear wave amplitude and steepness are obtained and discussed in the next section.) The difference between c and c_g decreases until it completely vanishes as the two roots coalesce at c_m. At this point expressions for the linear wave amplitude and steepness become singular, and the linear approximation breaks down. Based on the dispersion relation (2.5), if $U < c_m$, there are no solutions satisfying (2.9), and no wave can remain stationary on the stream. In this case there may exist local disturbances dying out away from the obstacle but no contribution to the asymptotic wave pattern. The disturbance level is then confined to a region about the pressure source represented by the obstacle and decays rapidly to zero with distance from it.

For the critical case, viscosity becomes important, and waves are damped very rapidly by it (for full details, see Lamb 1932, § 271).

For relatively deep water, two dimensionless parameters are defined for subsequent analysis – the Bond and the Froude number,

$$B = \frac{\tau}{\rho g (d-a)^2}, \qquad Fr = \frac{U}{\sqrt{g(d-a)}}. \tag{2.11}$$

Note that the Bond number is often defined as the inverse of B in the literature. For sufficiently large Froude numbers, inertial effects become dominant, and wave breaking may occur. However, nonlinear effects only arise when the inequality $a/d \ll 1$ is not satisfied. In addition an increase in the Bond number can reduce significantly the steepness of the surface waves formed due to the interaction of the cylinder with the current. A balance between inertial and surface tension effects may then occur such that wave breaking is postponed and in some cases annulled. For the study of pure gravity waves, the dimensionless parameters Fr and a/d are sufficient to define the regime of the problem, showing whether inertial and/or nonlinear effects play any role. When surface tension is added, B becomes the most important parameter for a general configuration. Depending on the value of B, capillary and/or gravity waves may appear at the free surface. However, the nature of the disturbances on the free surface also depends on the ratio between the stream velocity U and the minimum phase velocity c_m; B together with U/c_m is used in the subsequent analysis of the linear and nonlinear results.

3. Linear steady free-surface solution

The effects of surface tension on the disturbance produced by the flow of a uniform stream meeting a submerged cylindrical obstacle is investigated analytically on the basis of the linear steady solution described by Lamb (1932, § 247). The coordinate axes, x and y, have their origins located in the undisturbed level of the free surface. The centre of the cylinder is immediately below the origin at a position $\boldsymbol{x}_s = (0, -d)$. The velocity potential Φ satisfies Laplace's equation in the fluid domain excluding the singular point $\boldsymbol{x}_s$. At the far field, $\Phi \sim Ux$ as $|x| \to \infty$, for $-\infty < y \leqslant 0$; U represents the velocity of the stream and is assumed to be constant.

For a steady regime the kinematic and dynamic boundary conditions (2.1) simplify to

$$\frac{\partial \Phi}{\partial x}\frac{\partial \eta}{\partial x} = \frac{\partial \Phi}{\partial y}, \tag{3.1}$$

$$\frac{1}{2}\left[\left(\frac{\partial \Phi}{\partial x}\right)^2 + \left(\frac{\partial \Phi}{\partial y}\right)^2\right] + g\eta - \frac{\tau}{\rho}\frac{\partial^2 \eta}{\partial x^2}\left[1 + \left(\frac{\partial \eta}{\partial x}\right)^2\right]^{-3/2} = \frac{1}{2}U^2, \tag{3.2}$$

both valid on $y = \eta(x)$. Equation (3.2) now includes the surface tension term neglected by Lamb.

These boundary conditions can be linearized by assuming that the surface waves are sufficiently small. From perturbation theory, the velocity potential $\Phi(x, \eta)$ and the free-surface profile $\eta(x)$ can be written in terms of the algebraic expansions,

$$\Phi(x, \eta) = Ux + \epsilon \Phi_1 + \epsilon^2 \Phi_2 + \ldots, \qquad \eta(x) = \epsilon \eta_1 + \epsilon^2 \eta_2 + \ldots, \tag{3.3}$$

in which ϵ is a small parameter; the functions $\eta_i\,(i = 1, 2, \ldots)$ depends on x, while Φ_i depends on x and η. Substituting these approximations into (3.1) and (3.2) and

extracting the ϵ terms give

$$U\frac{\partial \eta}{\partial x} = \frac{\partial \phi}{\partial y}, \tag{3.4}$$

$$U\frac{\partial \phi}{\partial x} + g\eta - \frac{\tau}{\rho}\frac{\partial^2 \eta}{\partial x^2} = 0, \tag{3.5}$$

where, to simplify the notation, Φ_1 and η_1 were replaced by ϕ and η; ϕ denotes the velocity potential ϕ_s due to the dipole and satisfies Laplace's equation in the fluid domain, while at the far field $\phi \sim 0$ as $|x| \to \infty$, for $-\infty < y \leqslant 0$.

The flow about a circular horizontal cylinder is approximated by a dipole in a uniform stream flow. We assume that the radius a of the cylinder is small compared with the depth d of its axis. Then the velocity potential ϕ can be written as

$$\phi = Ux\left(1 + \frac{a^2}{r^2}\right) + \chi, \tag{3.6}$$

where $r(= \sqrt{x^2 + (y+d)^2})$ denotes the distance from the axis of the cylinder and χ is a harmonic function in all the fluid domain. Therefore, for $r = a$, $\partial\phi/\partial r = 0$, provided χ is negligible in the neighbourhood of the cylinder. Because of the reversibility of the flow, an antisymmetric velocity potential is required. Then χ is chosen as a Fourier integral of the form

$$\chi = \int_0^\infty \alpha(k)\, \mathrm{e}^{ky} \sin kx \, \mathrm{d}k, \tag{3.7}$$

with $\alpha(k)$ to be determined.

For positive values of $(y + d)$, expression (3.6) is equivalent to

$$\phi = Ux + Ua^2 \int_0^\infty \mathrm{e}^{-k(y+d)} \sin kx \, \mathrm{d}k + \chi. \tag{3.8}$$

Following Lamb's solution, the steady free-surface profile is chosen arbitrarily to be symmetric. Therefore it can be written as a cosine Fourier transform,

$$\eta(x) = \int_0^\infty \beta(k) \cos kx \, \mathrm{d}k, \tag{3.9}$$

in which $\beta(k)$ has to be determined.

Substituting the corresponding derivatives of (3.8) and (3.9) into the kinematic boundary condition (3.4) gives

$$-Ua^2\mathrm{e}^{-kd} + \alpha(k) = -U\beta(k). \tag{3.10}$$

For the dynamic boundary condition (3.5) we take only the first-order terms of the disturbance,

$$g\beta(k) + U^2a^2k\mathrm{e}^{-kd} + Uk\alpha(k) = -\frac{\tau}{\rho}k^2\beta(k). \tag{3.11}$$

This expression is independent of x. The right-hand side becomes negligible when surface tension effects are small. Combined with (3.10) this gives

$$\alpha(k) = -\frac{k+\kappa}{k-\kappa}Ua^2\mathrm{e}^{-kd}, \qquad \beta(k) = \frac{2a^2k\mathrm{e}^{-kd}}{k-\kappa}, \tag{3.12}$$

where

$$\kappa = \frac{g}{c^2}\left(1 + \frac{\tau}{\rho}\frac{k^2}{g}\right). \tag{3.13}$$

Note that κ is a function of k^2, which comes from the surface tension term included in the dispersion relation. It follows that the free-surface equation (3.9) has now a quadratic denominator in the integrand and can be rewritten as

$$\eta = -\frac{2\rho U^2 a^2}{\tau} \int_0^\infty \frac{k\mathrm{e}^{-kd}\cos kx}{(k-\kappa_g)(k-\kappa_\tau)}\mathrm{d}k, \tag{3.14}$$

where

$$\kappa_g = \frac{\rho U^2}{2\tau}\left(1 - \sqrt{1 - \frac{4\tau g}{\rho U^4}}\right), \qquad \kappa_\tau = \frac{\rho U^2}{2\tau}\left(1 + \sqrt{1 - \frac{4\tau g}{\rho U^4}}\right). \tag{3.15}$$

For real roots, κ_g and κ_τ represent the poles of integral (3.14), with $\kappa_\tau \geqslant \kappa_g$. These solutions correspond to waves travelling at the same phase speed, i.e. $c(\kappa_\tau) = c(\kappa_g) = U$, and can be associated to their group velocity through expression (2.8), which confirms that $c_g(\kappa_\tau) > U$ and $c_g(\kappa_g) < U$. Therefore one can conclude from group velocity concepts that capillary waves must appear ahead of the cylinder, while gravity waves must be downstream of it, supposing κ_τ and κ_g real.

In the limit, when τ goes to zero, expression (3.14) reduces to

$$\eta = 2a^2 \int_0^\infty \frac{k\mathrm{e}^{-kd}\cos kx}{k - g/U^2}\mathrm{d}k, \tag{3.16}$$

in accordance with Lamb's solution.

3.1. *Evaluation of the fourier integral*

The Fourier integral in (3.14) is indeterminate, but it can be evaluated in terms of its principal value (PV) for real values of κ_g and κ_τ, with $\kappa_g \neq \kappa_\tau$. By applying the residue theorem,

$$PV \int_0^\infty \frac{k\mathrm{e}^{-kd}\cos kx}{(k-\kappa_g)(k-\kappa_\tau)}\mathrm{d}k = \mathrm{Re}\left\{\pi\,\mathrm{i}\underset{k=\kappa_g,\kappa_\tau}{Res}\left[\frac{k\mathrm{e}^{\mathrm{i}kx-kd}}{(k-\kappa_g)(k-\kappa_\tau)}\right] - \int_0^\infty \frac{m\mathrm{e}^{-\mathrm{i}md-mx}}{(\mathrm{i}m-\kappa_g)(\mathrm{i}m-\kappa_\tau)}\mathrm{d}m\right\}, \tag{3.17}$$

which is valid for positive values of x. The integral on the right-hand side of (3.17) comes from completing the contour integration along the imaginary axis with $k = \mathrm{i}m$. Therefore,

$$\eta = \frac{2\rho U^2 a^2}{\tau}\left\{\int_0^\infty \frac{m\mathrm{e}^{-mx}\left[m(\kappa_g+\kappa_\tau)\sin md + (\kappa_g\kappa_\tau - m^2)\cos md\right]}{(m^2+\kappa_g^2)(m^2+\kappa_\tau^2)}\mathrm{d}m + \pi\left(\frac{\kappa_g\mathrm{e}^{-\kappa_g d}\sin\kappa_g x - \kappa_\tau\mathrm{e}^{-\kappa_\tau d}\sin\kappa_\tau x}{\kappa_g - \kappa_\tau}\right)\right\}, \qquad \text{for } x > 0. \tag{3.18}$$

The last term in (3.18) represents a stationary wavetrain obtained by the superposition of two wavetrains with lengths $2\pi/\kappa_g$ and $2\pi/\kappa_\tau$. Note that these waves maintain their position in space despite of the motion of the stream.

Taking the limit of (3.18) when τ goes to zero leads to

$$\eta = -2\pi\kappa a^2 \mathrm{e}^{-\kappa d}\sin\kappa x + 2a^2\int_0^\infty \frac{m\mathrm{e}^{-mx}\,(m\sin md + \kappa\cos md)}{m^2+\kappa^2}\mathrm{d}m, \tag{3.19}$$

valid for $x > 0$, which confirms Lamb's solution where, as here, $\kappa = g/U^2$. Note that the integral in (3.19) is equal to the real part of expression (3.16) with $k = \mathrm{i}m$.

Since the value of η in (3.9) is an even function of x, from its symmetry,

$$\eta = \frac{2\rho U^2 a^2}{\tau}\left\{\int_0^\infty \frac{m\mathrm{e}^{mx}\left[m(\kappa_g+\kappa_\tau)\sin md + (\kappa_g\kappa_\tau - m^2)\cos md\right]}{\left(m^2+\kappa_g^2\right)\left(m^2+\kappa_\tau^2\right)}\mathrm{d}m + \pi\left(\frac{\kappa_\tau \mathrm{e}^{-\kappa_\tau d}\sin\kappa_\tau x - \kappa_g \mathrm{e}^{-\kappa_g d}\sin\kappa_g x}{\kappa_g-\kappa_\tau}\right)\right\}, \qquad \text{for } x < 0. \tag{3.20}$$

Finally, analogous to Lamb's solution, on the disturbances represented by expressions (3.18) and (3.20) we superpose the stationary wavetrains

$$\eta = -2\pi\frac{\rho U^2 a^2 \kappa_g}{\tau\left(\kappa_g-\kappa_\tau\right)}\mathrm{e}^{-\kappa_g d}\sin\kappa_g x, \qquad \text{for } x > 0, \tag{3.21}$$

$$\eta = -2\pi\frac{\rho U^2 a^2 \kappa_\tau}{\tau\left(\kappa_g-\kappa_\tau\right)}\mathrm{e}^{-\kappa_\tau d}\sin\kappa_\tau x, \qquad \text{for } x < 0, \tag{3.22}$$

such that we annul the gravity waves occurring on the upstream side of the cylinder ($x > 0$) and the capillary waves downstream of it ($x < 0$), as it is required from the group velocity for a physical solution.

For $\kappa_g = \kappa_\tau$, the Fourier integral in (3.14) has a second-order pole integrand and cannot be evaluated. Lamb (1932) uses artificial damping through viscosity to move poles off the axis, and in this critical case this shows that damping from viscous forces is a dominant effect. For complex roots, $\kappa_g = \overline{\kappa_\tau}$. Then the integrand in (3.14) becomes non-singular, simplifying to

$$\eta = -\frac{2\rho U^2 a^2}{\tau}\int_0^\infty \frac{k\mathrm{e}^{-kd}\cos kx}{[k-\mathrm{Re}(\kappa_\tau)]^2 + [\mathrm{Im}(\kappa_\tau)]^2}\mathrm{d}k, \tag{3.23}$$

which is an improper integral. With a suitable change of variables, the infinite range of integration can be mapped into a finite one, such that this integral can be evaluated numerically (see Press *et al.* 1986, p. 115).

3.2. *Linear results*

Linear results are presented in figure 3 for different values of the Bond number B. For each case the location of the poles κ_g and κ_τ with respect to the dispersion relation is shown in figure 4, with the horizontal dotted lines representing where $c(\kappa_g) = c(\kappa_\tau) = U$. The parameters U, k, k_m, c, c_m and c_g are presented in the dimensionless form. Then the ratio U/c_m is equal to the non-dimensional ratio $Fr/(4B)^{1/4}$; for a fixed stream velocity the ratio U/c_m decreases as B increases.

The group velocity is represented by the dashed lines in figure 4. It is important to note that when the stream velocity is greater than the minimum phase speed, i.e. $U > c_m$ (cases *b–d*), $c_g(\kappa_g) < c(\kappa_g)$ and $c_g(\kappa_\tau) > c(\kappa_\tau)$. Since $c(\kappa_g) = c(\kappa_\tau) = U$, one

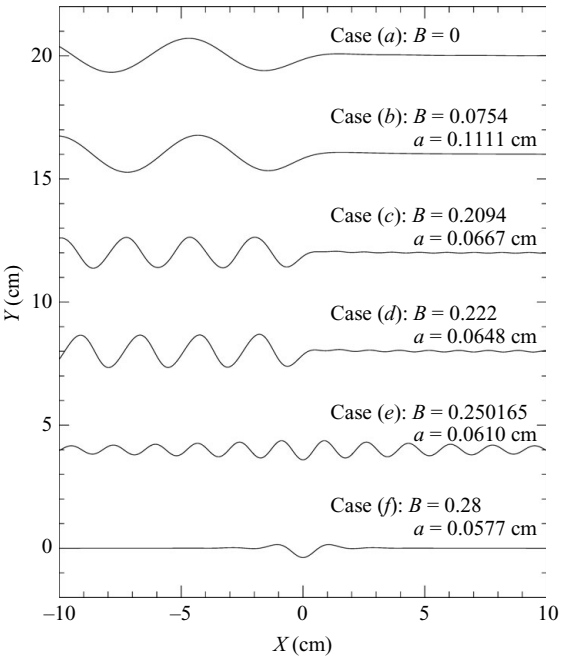

FIGURE 3. Linear steady solutions for different values of $(d-a)$: (a) ∞ $(\tau = 0)$; (b) 1.0 cm; (c) 0.6 cm; (d) 0.583 cm; (e) 0.549 cm; (f) 0.519 cm. For all cases $a/d = 1/10$, $U = -1$ and $Fr = 0.75$. Except in case (e), surface displacement is vertically exaggerated 10 times.

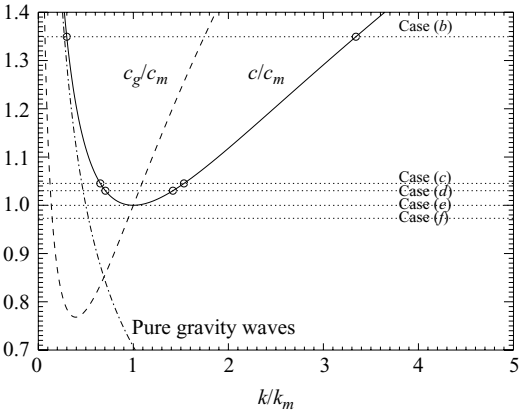

FIGURE 4. Location of the poles κ_g and κ_τ with respect to the phase and group velocity; $k_m = B^{-1/2}$; $c_m = (4B)^{1/4}$; U, k, k_m, c, c_m and c_g are dimensionless quantities.

can confirm from group velocity concepts the results presented in figure 3: capillary waves are formed upstream of the cylinder, while gravity waves appear downstream. Note also that the ripples formed upstream of the cylinder become more prominent as B increases. Wave amplitudes and steepnesses according to linear theory are plotted against c/c_m in figure 5.

For all the cases here presented the ratio a/d is kept constant and equal to 1/10. As discussed before, for larger values of a/d, waves become 'steeper', and nonlinear

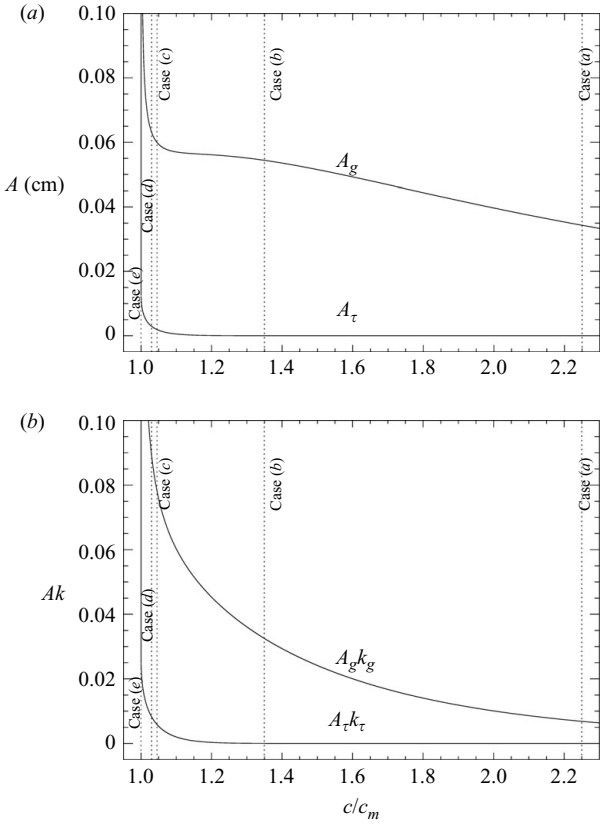

FIGURE 5. Variation of (*a*) amplitude and (*b*) wave steepness as a function of c/c_m according to linear theory.

phenomena may arise at the water surface. For a constant d, as the ratio a/d increases, the depth of submergence $(d-a)$ decreases and, therefore, B increases, with surface tension effects becoming more important. Excepting case (*e*), all the free-surface profiles are vertically exaggerated 10 times. Note also that x and y are non-dimensionalized by the characteristic length scale $(d-a)$ in case (*a*) of figure 3; no surface tension effects are included in this case. The radius of the cylinder a is also provided for each case.

For sufficient large values of $(d-a)$, surface tension effects become negligible, i.e. $B \to 0$; the solution then approaches the form of a sinusoidal wavetrain with wavelength $2\pi U^2/g$, located downstream of the cylinder as predicted Lamb (see figure 3, case *a*). This means that in the limit, κ_g tends to g/U^2, with no contribution coming from the capillary branch. This is confirmed from figure 4, which shows that the solid curve, representing the capillary–gravity waves, approaches the pure gravity wave solution (dash-dotted line) for increasing values of c. For $k < k_m/10$ and $c > 2.25c_m$, gravity dominates the free-surface motion. In addition it is possible to see from figure 5 that for $c > 2.25c_m$, wave amplitudes and steepnesses keep decreasing. This means that disturbances become less prominent for increasing values of $(d-a)$, as expected.

In figure 3, cases (*b*)–(*d*) correspond to the surface profiles for real values of κ_g and κ_τ. For $B = 0.0754$ (case *b*), $\kappa_g = 1.1$ and $\kappa_\tau = 12.2$, and the solution is close to a pure gravity wavetrain. Surface tension effects are very small in this case with κ_g very close to the gravity wave limit (see figure 4). In fact figure 5(*b*) reveals that these 'gravity-like' waves are 'steeper' than the latter. Furthermore figure 5(*a*) shows that the capillary wave amplitudes are almost too small to be noticed in figure 3.

As the two poles κ_g and κ_τ approach each other, wave amplitudes tend to increase at both sides of the cylinder (see figure 5*a*), and so nonlinear effects may become important. An increase in wave steepness is also observed with small-scale ripples becoming visible ahead of the cylinder (see figure 3, cases *c* and *d*). For instance, case (*c*) has a wave height of approximately 0.04 mm upstream of the cylinder and 1.2 mm downstream of it. As discussed before, the appearance of capillary and gravity waves situated respectively upstream and downstream of the cylinder is predicted from group velocity concepts, with the results being confirmed by natural observations.

Wave steepnesses continue to grow on both sides as we approach c_m (see figure 5*b*), with the solution becoming singular when the two poles coalesce. With respect to the group velocity, figure 4 shows that $c_g(\kappa_g)$ approaches $c_g(\kappa_\tau)$ as the stream velocity U becomes closer to the minimum phase velocity c_m until $U = c_m = c(\kappa_g) = c(\kappa_\tau)$. Note that for a constant stream velocity, $U/c_m \to 1$ as $B \to Fr^4/4$. In figure 3, cases (*e*) and (*f*) show the surface profiles for $U < c_m$, i.e. when κ_g and κ_τ become complex. Disturbances become symmetric with amplitudes decaying exponentially in both $\pm x$ directions. This is confirmed by expression (3.23) in which η is an even function of x. In case (*e*) the stream velocity U is very close to the minimum phase velocity ($U/c_m = 0.9998$) with waves becoming very steep. No vertical exaggeration was used in this case. Nonlinear effects may play an important role in this region with the linear solution becoming inaccurate.

As B increases, with $B > Fr^4/4$, the solution behaves as a local disturbance, decaying rapidly to zero with distance from the cylinder (see figure 3, case *f*). According to figure 4, no real steady solution with waves at ∞ exists for the phase speed. However, for the group velocity two solutions are possible when $c_m > U > c_{g_m}$, though waves cannot be steady in this case. Thus for an initial-value problem waves can radiate away. For $c_m > U > c_{g_m}$ waves do exist, and some are swept downstream of the cylinder, while waves of all frequencies are radiated away for $U < c_{g_m}$. In the following section the nonlinear numerical model is employed with the aim of shedding further light on the behaviour of the solution in the neighbourhood of c_m.

It is important to note that the radius of the cylinder is a parameter of the problem that does have some influence on the waves. In the cases presented in figure 3, a is small compared with the wavelength of the minimum group velocity, i.e. $\lambda_{g_m} = 2\pi/k_{g_m} = 1.329$ cm. The effects for larger values of a are of interest and are presented in the next section.

4. Fully nonlinear results

The numerical results here presented are obtained by applying the fully nonlinear unsteady boundary-integral scheme described in § 2.1. When running the code the input data is set up such that $(d - a)$ corresponds to the characteristic length scale of the problem. The corresponding parameters that define the underlying flow, i.e. the stream velocity U, the depth of submergence d and the radius of cylinder a, are also provided. The dipole is supposed to be at a fixed position in time. The initial conditions employed in the calculations are a flat free surface or the linear

steady solutions derived in the previous section. Small disturbances associated to the impulsive motion of the problem may appear in the nonlinear results. In these cases long-run computations are used with the aim of obtaining quasi-steady profiles. All the presented numerical simulations were computed on a Sun Ultra 2/200.

4.1. *Pure gravity waves*

Before analysing the effects of surface tension at the free surface, consider the case in which gravity dominates the fluid motion. For this situation the dispersion relation is given by $c = \pm(g/k)^{1/2}$, with no minimum phase velocity. For sufficiently small values of a/d, nonlinear effects are negligible, and Lamb's linear solution gives a good approximation for the free-surface elevation. Figure 6(a) shows with a vertical exaggeration of 50:1 the stacked free-surface displacement induced by a stream flow ($U = -0.6$) interacting with a cylinder ($a/d = 1/10$). The initial starting profile is that of an undisturbed flat free surface. The underlying motion is switched on at time $t = 0$, generating unsteady waves that propagate in the $-x$ direction. A sinusoidal wavetrain with wavelength $2\pi U^2/g$ is soon formed downstream of the cylinder, as predicted by linear theory. As the ratio a/d increases, nonlinear effects become important. The solution then may involve highly non-sinusoidal or breaking waves.

Figure 6(b) shows the nonlinear free-surface displacement for $a/d = 1/5$ and $U = -0.6$. Waves are formed downstream of the cylinder and are noticeably affected by nonlinearity in this case. For bigger values of a/d, disturbances induced by the underlying flow are unsteady and strong enough to cause wave breaking (see figure 6c). For these cases the nonlinear computations do not reach a stationary profile after a certain time. Breaking occurs isolated downstream of the cylinder, in a region very close to it. This result confirms the investigations of Tuck (1965) and Dagan (1971) who suggested that wave breaking does occur when a/d is not sufficiently small. In these cases linear theory fails and Lamb's classical solution of a sinusoidal wavetrain downstream of the cylinder does not apply.

Figure 7 compares the linear stationary free-surface profiles with quasi-steady nonlinear results for two different values of a/d, neglecting surface tension effects. As expected a good agreement between linear and nonlinear results is found in figure 7(a, b). In these cases the cylinder is sufficiently far from the free surface for no nonlinear interactions to take place. On the other hand discrepancies between the profiles can be clearly noticed in case (c). In this case the cylinder becomes closer to the free surface as a increases for a fixed d. In particular, case (c) shows that the nonlinear result becomes 'steeper' than the linear one, with sharper crests and shorter wavelengths.

4.2. *Capillary–gravity waves*

With the introduction of surface tension the linear dispersion relation has a minimum phase speed c_m which defines a region in which waves do appear, i.e. $U > c_m$. Two real roots then exist, and for $a/d \ll 1$, linear theory determines accurately the wave properties of the problem. However, if the ratio a/d increases, nonlinear effects may become important. If that is the case, then the free-surface profile is distorted, and wave breaking may occur. For a constant d, as a/d assumes larger values, B also increases, and thus surface tension effects may postpone wave breaking. Nonlinearity may also affect the free-surface profile for values of $U < c_m$. Figure 8 shows the location of the nonlinear cases studied in this section with respect to the phase and group velocity of capillary–gravity waves. The fully nonlinear unsteady boundary-integral method introduced in § 2 is here employed taking into account the effects of surface tension. Special attention is directed to the cases in which $U < c_m$, i.e.

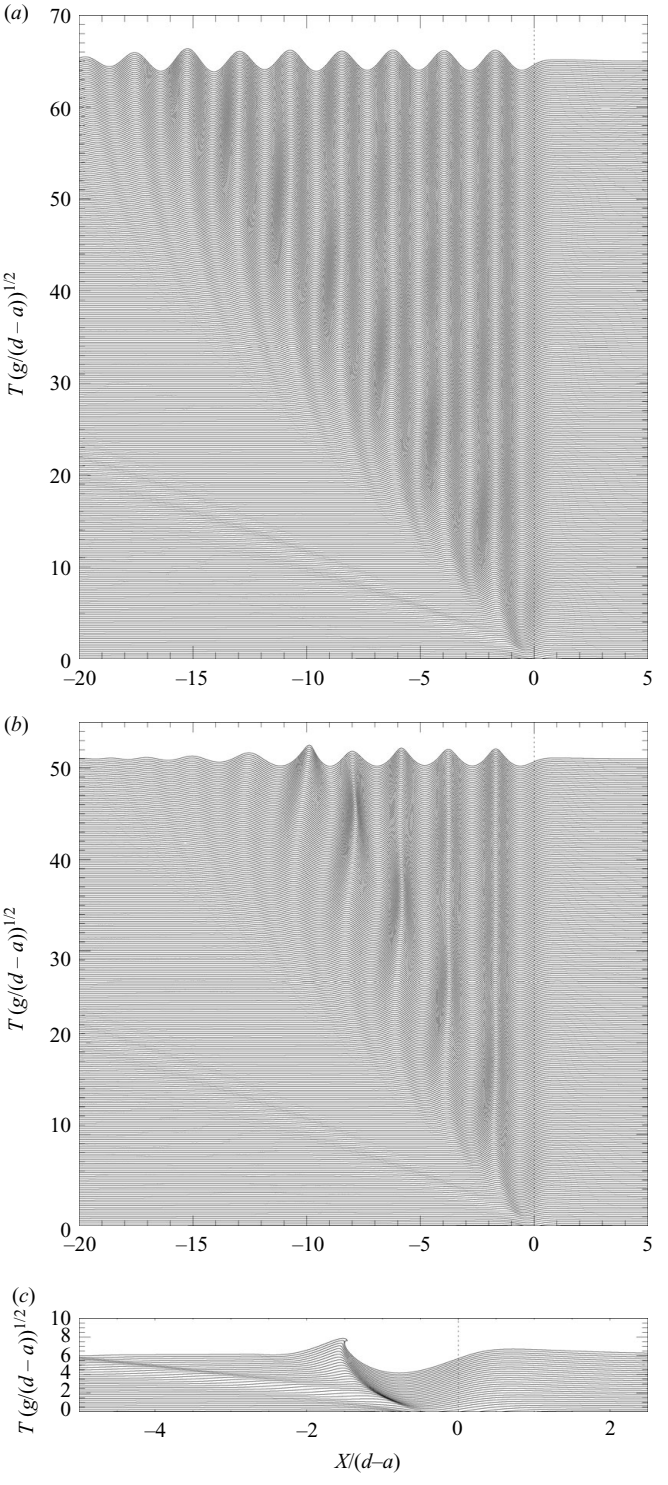

FIGURE 6. Fully nonlinear results for a uniform stream flow ($U = -0.6$) interacting with a submerged cylinder: (*a*) $a/d = 1/10$, vertical exaggeration 50:1; (*b*) $a/d = 1/5$, vertical exaggeration 10:1; (*c*) $a/d = 1/3$, vertical exaggeration 10:1, $t_{breaking} = 6.0$. For all cases $B = 0$ and $Fr = 0.44$.

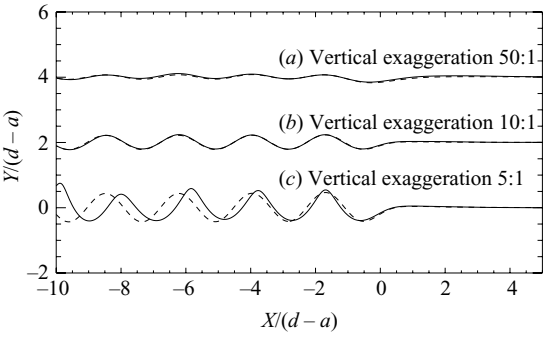

FIGURE 7. Comparison between nonlinear (——) and linear steady results (– – –) with no surface tension ($B = 0$): (*a*) $a/d = 1/20$; (*b*) $a/d = 1/10$; (*c*) $a/d = 1/5$. For all cases $U = -0.6$ and $Fr = 0.44$.

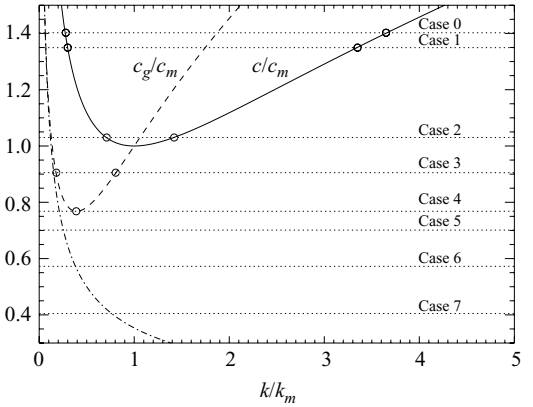

FIGURE 8. Location of the fully nonlinear results with respect to the phase and group velocity of capillary–gravity waves. The dash-dotted line represents the group velocity of pure gravity waves; $k_m = B^{-1/2}$; $c_m = (4B)^{1/4}$; U, k, k_m, c, c_m and c_g are dimensionless quantities.

$B > Fr^4/4$, with the ratio a/d assuming values sufficiently large for nonlinear effects to take place.

Figure 9(*a*, *b*) compares quasi-steady nonlinear results with linear steady solutions for cases 1 ($B = 0.0754$) and 2 ($B = 0.2218$) respectively, where $U > c_m$ (see figure 8). In these cases a flat free surface was used as the initial condition of the boundary value problem. Note that in both cases $a/d = 1/10$, and a vertical exaggeration of 10:1 was used. As expected a good agreement was observed between the linear and nonlinear results, with 'gravity-like' waves being formed downstream of the cylinder and 'capillary-like' waves ahead of it, which are visible only in case 2 in which surface tension effects become more prominent ($B = 0.2218$). In both cases the nonlinear wave amplitudes give accurate linear solutions (see figure 5). When the ratio a/d is increased to 1/3, keeping U/c_m and B with the same values, nonlinear effects take over, and wave breaking occurs in both cases within very short times.

According to linear theory, if the value of U/c_m decreases, such that $U < c_m$, no real steady solution with waves exists for the phase speed, with only a local disturbance being predicted (see for instance figure 3, cases *e* and *f*). However two roots exist for the group velocity if $c_m > U > c_{g_m}$, which may be associated to unsteady waves.

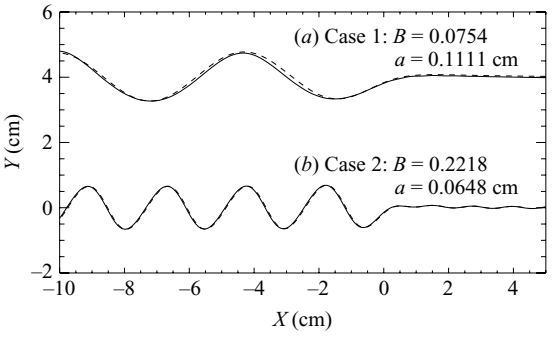

FIGURE 9. Comparison between quasi-steady nonlinear results (——) and linear stationary solutions (– – –): (*a*) $U/c_m = 1.3494$, $(d-a) = 1$ cm; (*b*) $U/c_m = 1.0301$, $(d-a) = 0.583$ cm. In the cases presented here $a/d = 1/10$, $U = -1$, $Fr = 0.75$ and $c_m = (4B)^{1/4}$; U and c_m are dimensionless quantities. Vertical exaggeration is 10:1.

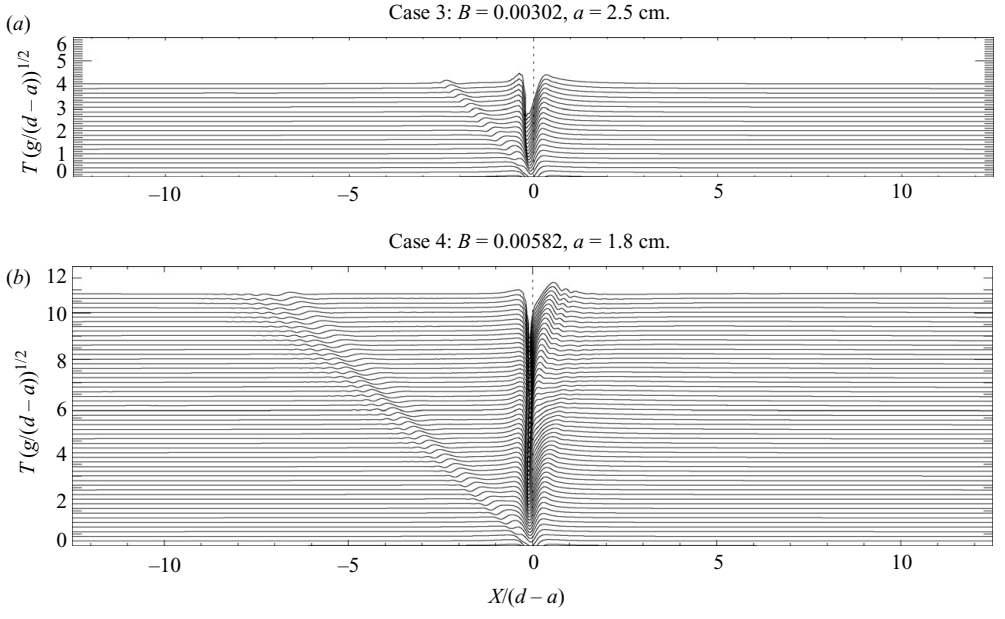

FIGURE 10. Fully nonlinear results for a uniform stream flow interacting with a submerged cylinder: (*a*) $U/c_m = 0.9052$, $(d-a) = 5.0$ cm, $t_{breaking} = 4.0$; (*b*) $U/c_m = 0.7681$, $(d-a) = 3.6$ cm, $t_{breaking} = 10.8$. In this case $a/d = 1/3$, $U = -0.3$, $Fr = 0.7$ and $c_m = (4B)^{1/4}$; U and c_m are dimensionless quantities. Vertical exaggeration is 25:1.

Indeed the unsteady nonlinear computed cases 3 and 4 show that wave breaking occurs in this region. In fact case 3 has the calculations stopped at a shorter time ($t_{breaking} = 4.0$), supposing $B = 0.00302$, $a/d = 1/3$ and $U/c_m = 0.9052$ (see figure 10*a* for details). Figure 10(*b*) illustrates case 4, for which $B = 0.00582$, $a/d = 1/3$ and $U/c_m = 0.7681$. The time at which breaking occurs has now increased to 10.8. Since B is very small in both cases, surface tension effects are less prominent. The initial condition here used corresponds to the linear steady solution obtained in § 3. Because of the impulsive starting motion some capillary–gravity waves are visible propagating

in the $-x$ direction. Waves are also formed ahead of the cylinder, but these are 'trapped' by the adverse stream flow U, with energy building up there until wave breaking occurs. Note that for case 4, U is very close to c_{g_m}.

For $U < c_{g_m}$ wave breaking was no longer observed in the unsteady nonlinear computations for constants a/d $(= 1/3)$ and U $(= -0.3)$. In fact, as B increases, U/c_m decreases, and the capillary–gravity waves generated ahead of the cylinder are no longer 'trapped' by the adverse current and now radiate upstream of the cylinder. This feature was observed in cases 5–7 for long computational runs (see figure 11), where $B = 0.00838$, 0.01885 and 0.0754, respectively. As B increases, surface tension effects become more important. Indeed capillary–gravity waves are formed as the underlying motion is switched on at time $t = 0$, generating unsteady waves that propagate in the $-x$ and $+x$ directions. The group velocity of the waves formed downstream of the cylinder is augmented by the following current and radiates away. On the other hand the group velocity of the capillary–gravity waves formed ahead of the cylinder is reduced by the adverse stream flow, as can be seen from figure 11(a, b). As U/c_m keeps decreasing (since B increases), the stream velocity has less effect on the capillary–gravity waves generated until they are totally radiated away in both x directions, as shows figure 11(c).

Comparisons between the linear and nonlinear wave profiles for cases 6 and 7 are presented in figure 12(a, b). A vertical exaggeration of 10:1 was employed at the free-surface elevation in these cases. The linear steady solution behaves as a local disturbance, decaying rapidly to zero with distance from the cylinder, and thus it is used as the initial condition of the fully nonlinear problem. A good agreement was found between the linear and nonlinear results. Note also that the radius a is now not very different from the wavelength of the minimum group velocity $\lambda_{g_m} = 1.329$cm. As a increases, the free surface becomes more disturbed until wave breaking occurs (see figures 10 and 11).

Short capillary waves with wavelengths of several millimetres can often be seen near the crests of steep gravity waves with lengths between 5 and 25 cm. This phenomenon was also observed in the unsteady nonlinear computations. Figure 13 shows the formation of 'parasitic' capillary waves near the crest of gravity waves formed downstream of the cylinder. In this case $B = 0.00378$, $a/d = 1/5$ and $U/c_m = 1.4023$. Because of the high curvature at the crest of the gravity wave, surface tension effects become locally important in this case, even though B assumes a small value. The capillary waves formed upstream of the cylinder have a very small amplitude and cannot be noticed in figure 13. Note that the appearance of capillary waves downstream of the cylinder is essentially a nonlinear phenomenon which is not predicted from group velocity concepts. The time at which breaking occurs is equal to 14.2.

5. Summary

The interaction between a free-surface flow with surface tension and an approximately circular, horizontal cylinder has been investigated. The present work was motivated by several authors who had studied the effects of nonlinearity in the classical linear solution given by Lamb (1913) but without considering capillary action. A fully nonlinear model which includes surface tension and a dipole in a stream flow was developed with the aim of understanding the behaviour of the free-surface flow. A linear steady solution including surface tension effects was derived

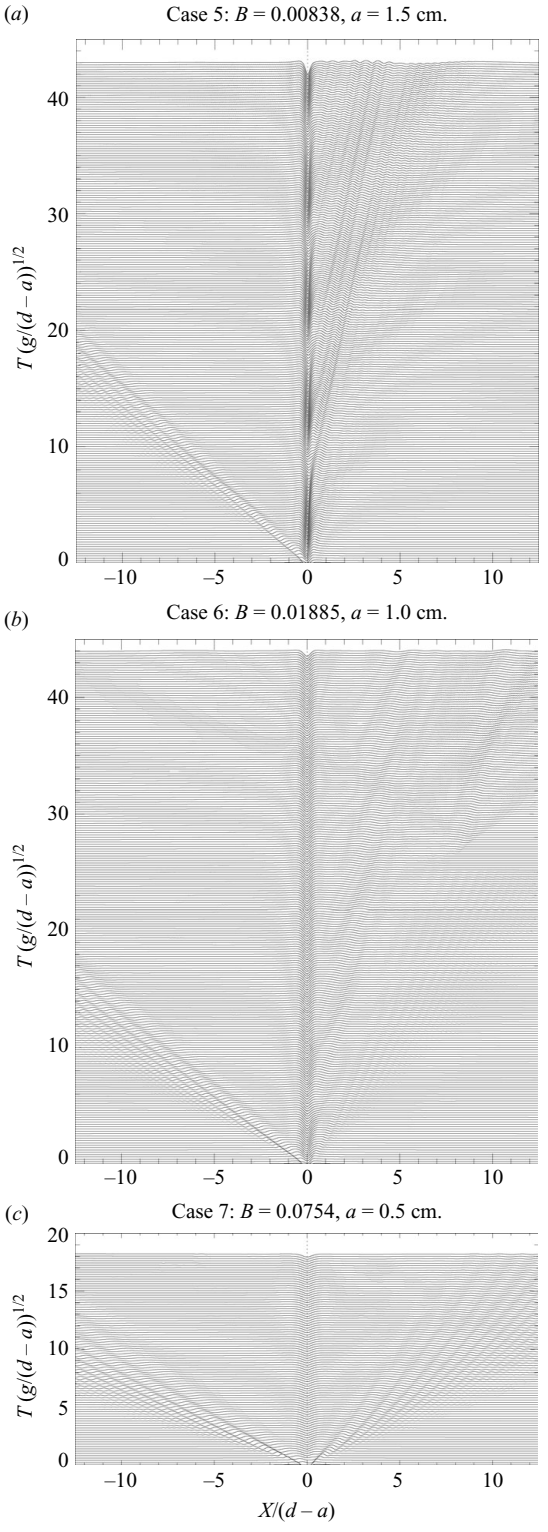

FIGURE 11. Fully nonlinear results for a uniform stream flow ($U = -0.3$) interacting with a submerged cylinder ($a/d = 1/3$, $Fr = 0.7$): (*a*) $U/c_m = 0.7012$, $(d - a) = 3$ cm. (*b*) $U/c_m = 0.5725$, $(d - a) = 2$ cm. (*c*) $U/c_m = 0.4048$, $(d - a) = 1$ cm. $c_m = (4B)^{1/4}$; U and c_m are dimensionless quantities. Vertical exaggeration is 25:1.

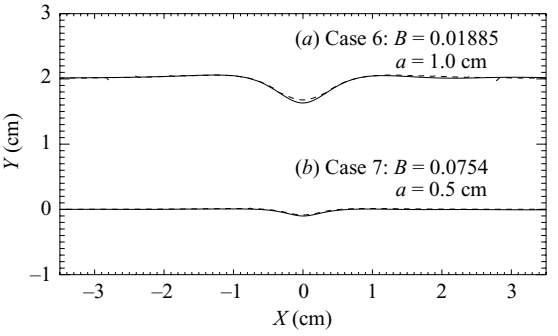

FIGURE 12. Comparison between nonlinear (——) and linear results (– – –): (*a*) $U/c_m = 0.5725$, $(d-a) = 2$ cm; (*b*) $U/c_m = 0.4048$, $(d-a) = 1$ cm. For all cases $a/d = 1/3$, $U = -0.3$, $Fr = 0.67$ and $c_m = (4B)^{1/4}$; U and c_m are dimensionless quantities. Disturbances are vertically exaggerated 10 times.

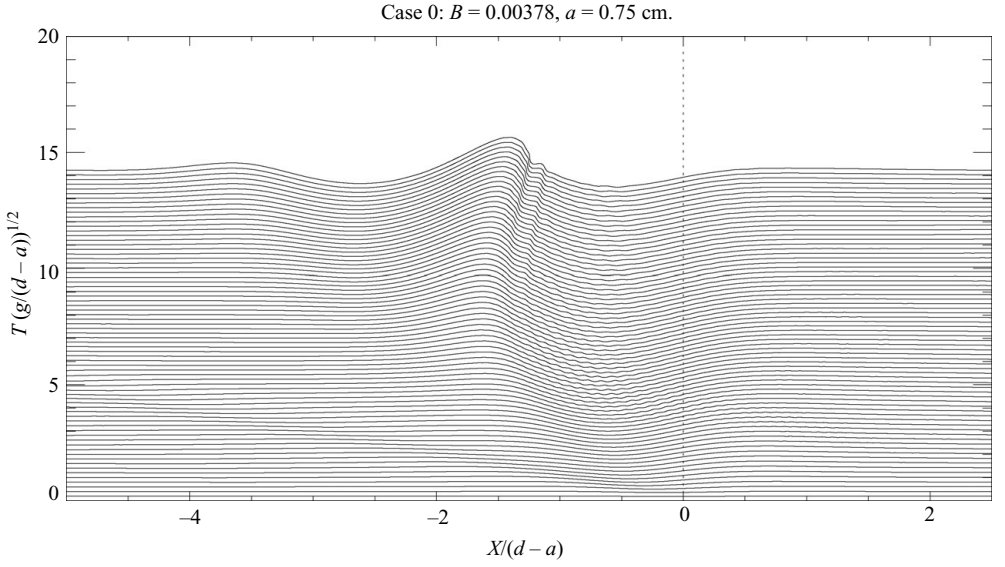

FIGURE 13. Fully nonlinear results for a uniform stream flow interacting with a submerged cylinder: $U/c_m = 1.4023$, $(d-a) = 3.0$ cm. In this case $a/d = 1/5$, $U = -0.6$, $Fr = 0.44$ and $c_m = (4B)^{1/4}$; U and c_m are dimensionless quantities; $t_{breaking} = 14.2$. Vertical exaggeration is 10:1.

and employed as the initial condition of the nonlinear model in some of the computed cases.

For sufficiently small values of a/d, a good agreement between the quasi-steady nonlinear numerical results and the linear steady solutions is obtained for both pure gravity and capillary–gravity waves. However, as the ratio a/d increases, nonlinearity starts to play an important role. For pure gravity waves, the fully nonlinear results show that waves become 'steeper', with sharper crests and shorter wavelengths, with wave breaking occurring when larger values of a/d are imposed.

With the introduction of surface tension, the numerical simulations have shown that wave breaking also occurs for sufficiently large values of a/d, but now this also depends on the Bond number B. As B increases, surface tension effects become more

prominent; capillarity can then significantly reduce the steepness of the free-surface disturbances when it precludes the formation of steady waves. For $U > c_{g_m}$ wave breaking was observed in all the computed cases when the inequality $a/d \ll 1$ was not satisfied. For $U < c_{g_m}$, an interesting feature was found: capillary–gravity waves are formed upstream of the cylinder. According to linear theory, only a local disturbance which decays rapidly to zero with distance from the centre of the cylinder should happen in this case. However in an initial-value problem waves can radiate away. As U/c_m decreases, with values smaller than the minimum group velocity c_{g_m}, waves of all frequencies are radiated upstream and downstream. Then the nonlinear result approaches the linear steady solution of a local disturbance at the free surface.

R. M. M. acknowledges the financial support through CAPES, the Brazilian agency for postgraduate education, and CNPq, the national research and development council (contract number 62.0018/2003-8-PADCT III / FAPERJ). The author is grateful for the referees' comments and also for the extensive review of Dr R. Porter from University of Bristol and Dr J. T. A. Chacaltana from Federal University of Espírito Santo. This paper is dedicated to the memory of Professor D. H. Peregrine.

REFERENCES

Batchelor, G. K. 1967 *An Introduction to Fluid Dynamics*. Cambridge University Press.

Ceniceros, H. D. & Hou, T. Y. 1999 Dynamic generation of capillary waves. *Phys. Fluids* **11**, 1042–1050.

Chen, B. & Saffman, P. G. 1980 Steady gravity–capillary waves on deep water. Part II. Numerical results for finite amplitude. *Stud. Appl. Math.* **62**, 95–111.

Crapper, G. D. 1970 Non-linear capillary waves generated by steep gravity waves. *J. Fluid Mech.* **40**, 149–159.

Dagan, G. 1971 Free-surface gravity flow past a submerged cylinder. *J. Fluid Mech.* **49**, 179–192.

Dias, F. & Kharif, C. 1999 Nonlinear gravity and capillary–gravity waves. *Annu. Rev. Fluid Mech.* **31**, 301–346.

Dold, J. W. 1992 An efficient surface-integral algorithm applied to unsteady gravity waves. *J. Comput. Phys.* **103**, 90–115.

Dommermuth, D. 2000 The initialization of nonlinear waves using an adjustment scheme. *Wave Mot.* **32**, 307–317.

Forbes, L. K. 1983 Free-surface flow over a semicircular obstruction, including the influence of gravity and surface tension. *J. Fluid Mech.* **127**, 283–297.

Grandison, S. & Vanden-Broeck, J.-M. 2006 Truncation approximations for gravity–capillary free-surface flows. *J. Engng Math.* **54**, 89–97.

Havelock, T. H. 1926 The method of images in some problems of surface waves. *Proc. R. Soc. Lond.* A **115**, 268–280.

Havelock, T. H. 1936 The forces on a circular cylinder submerged in a uniform stream. *Proc. R. Soc. Lond.* A **157**, 526–534.

Hogan, S. J. 1979 Some effects of surface tension on steep water waves. *J. Fluid Mech.* **91**, 167–180.

Hogan, S. J. 1980 Some effects of surface tension on steep water waves. Part 2. *J. Fluid Mech.* **96**, 417–445.

Hogan, S. J. 1981 Some effects of surface tension on steep water waves. Part 3. *J. Fluid Mech.* **110**, 381–410.

Hogan, S. J. 1983 Energy flux in capillary–gravity waves. *Phys. Fluids* **26**, 1206–1209.

Jervis, M. T. 1996 Some effects of surface tension on water waves and water waves at a wall. PhD thesis, University of Bristol, Bristol.

Lamb, H. 1913 On some cases of wave-motion on deep water. *Ann. Mat.* **3**, xxi, 237.

Lamb, H. 1932 *Hydrodynamics*, 6th edn. Cambridge University Press.

Longuet-Higgins, M. S. 1963 Generation of capillary waves by steep gravity waves. *J. Fluid Mech.* **16**, 138–159.

Longuet-Higgins, M. S. & Cokelet, E. D. 1976 The deformation of steep surface waves on water. Part I. A numerical method of computation. *Proc. R. Soc. Lond.* A **350**, 1–26.

Maleewong, M., Grimshaw, R. & Asavanant, J. 2005 Free surface flow under gravity and surface tension due to an applied pressure distribution. Part II. Bond number less than one-third. *Eur. J. Mech.* B **24**, 502–521.

Milewski, P. A. & Vanden-Broeck, J.-M. 1999 Time dependent gravity–capillary flows past an obstacle. *Wave Mot.* **29**, 63–69.

Moreira, R. M. 2001 Nonlinear interactions between water waves, free surface flows and singularities. PhD thesis, University of Bristol, Bristol.

Perlin, M. & Schultz, W. W. 2000 Capillary effects on surface waves. *Annu. Rev. Fluid Mech.* **32**, 241–274.

Press, W. H., Flannery, B. P., Teukolsky, S. A. & Vetterling, W. T. 1986 *Numerical Recipes – the Art of Scientific Computing*. Cambridge University Press.

Rottman, J. W. & Olfe, D. B. 1979 Numerical calculations of steady gravity–capillary waves using an integro-differential formulation. *J. Fluid Mech.* **94**, 777–793.

Ruvinsky, K. D., Feldstein, F. I. & Freidman, G. I. 1991 Numerical simulation of the quasi-stationary stage of ripple excitation by steep gravity–capillary waves. *J. Fluid Mech.* **230**, 339–353.

Ruvinsky, K. D. & Freidman, G. I. 1981 The generation of capillary–gravity waves by steep gravity waves. *Izv. Atmos. Ocean. Phys.* **17**, 548–553.

Schwartz, L. W. & Vanden-Broeck, J.-M. 1979 Numerical solution of the exact equations for capillary–gravity waves. *J. Fluid Mech.* **95**, 119–139.

Scullen, D. & Tuck, E. O. 1995 Nonlinear free-surface flow computations for a submerged cylinder. *J. Ship Res.* **39**, 185–193.

Tanaka, M., Dold, J. W., Lewy, M. & Peregrine, D. H. 1987 Instability and breaking of a solitary wave. *J. Fluid Mech.* **185**, 235–248.

Tuck, E. O. 1965 The effect of nonlinearity at the free surface on flow past a submerged cylinder. *J. Fluid Mech.* **22**, 401–414.

Tyvand, P. A. & Miloh, T. 1995*a* Free surface flow due to impulsive motion of a submerged circular cylinder. *J. Fluid Mech.* **286**, 67–101.

Tyvand, P. A. & Miloh, T. 1995*b* Free surface flow generated by a small submerged circular cylinder starting from rest. *J. Fluid Mech.* **286**, 103–116.

Vanden-Broeck, J.-M. 2002 Wilton ripples generated by a moving pressure distribution. *J. Fluid Mech.* **451**, 193–201.

Whitham, G. B. 1999 *Linear and Nonlinear Waves*. John Wiley.

Wilton, J. R. 1915 On ripples. *Phil. Mag.* **29**, 688–700.